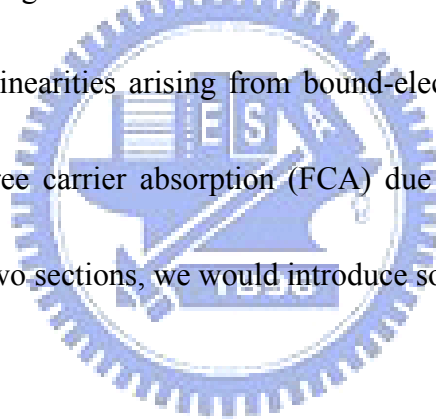


# Chapter 1 Introduction

## 1-1 Applications of optical nonlinearities

The nonlinear optical properties in semiconducting materials are being widely studied as potential applications to various optical devices. The determination of optical nonlinearities and their response times in semiconductor is great important to the practical applications of all-optical switching elements and optical limiting devices. Usually, the optical nonlinear response in the transparent region of semiconductors can be classified into two categories, namely, (1) third-order nonlinearities arising from bound-electronic effects and two photon absorption (TPA) and (2) free carrier absorption (FCA) due to the photoexcitation of free carriers. In the following two sections, we would introduce some important applications.



### 1-1-1 Optical switching

There is a growing interest in the development of optical switching and signal-processing devices for use in future systems despite of the continued progress in electronics technology. One reason for this interest is the potential of all-optical switching devices to operate at speeds and bandwidths much greater than those possible with electronic devices, because the response time of optical nonlinearities in the transparency region is essentially instantaneous. In recent years, considerable research has gone into the study of all-optical switching devices

in waveguides [1].

For a material with a three-level system, a pump and probe technique can be utilized to demonstrate an all-optical switching which is based on nonlinear absorption. Figure 1-1 shows the schematic diagram illustrates the switches processes. The probe beam of wavelength 815 nm is absorbed by the intermediate state when the pulsed pump beam is off. The transmission intensity of the probe beam is low because of high linear absorption, i.e., it is in the off state. Exposure of the sample to the pump beam (665 nm) causes the depopulation of the ground state and increased population of the intermediate state. This induces a bleaching of the ground state to the intermediate state, causing the transmission intensity of the probe beam to increase, i.e., it is in the on state [2].

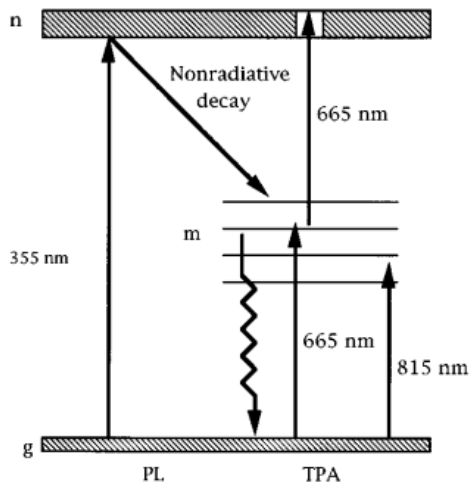
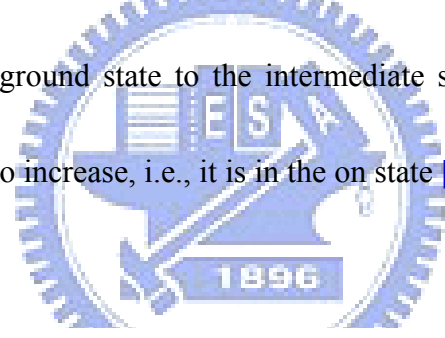


Fig. 1-1 A schematic diagram illustrates the two photon absorption and switches processes.

### 1-1-2 Optical limiting

Nonlinear optical materials with large intensity-induced refractive index and absorption change have strong potential application in the design of the optical limiters, which can protect optical sensors and human eyes from laser damages. In the optical limiting, the absorption of material increases following the increasing of exciting intensity. This behavior is attributed to a reverse saturation mechanism which results from population of an excited state that has greater absorption cross section than that of the ground state. The increase of the absorption coefficient of a nonlinear optical medium with increasing amount of incident light intensity can be used to limit the amount of energy transmitted by the medium, which could be shown in Fig. 1-2. The optical limiting in inorganic clusters is caused by strong nonlinear refraction, whereas the optical limiting in semiconductor structures is governed by two-photon absorption.

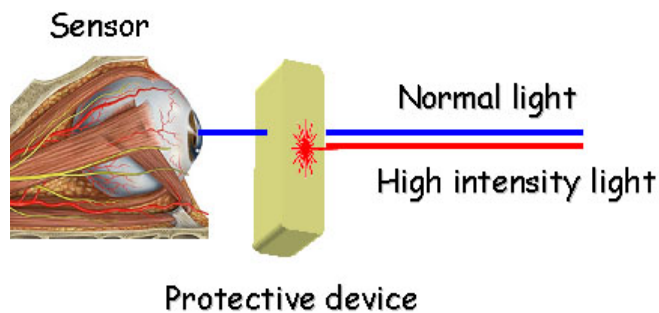


Fig. 1-2 A schematic diagram illustrates the process of optical limiting.

## 1-2 Measurement techniques of optical nonlinearities

In this section, we introduce two common experimental techniques for optical nonlinearities measurement. They are four-wave mixing and single beam Z-scan. These methods could measure nonlinear refraction and nonlinear absorption and would be described below. Their merits and drawbacks will also be compared.

### 1-2-1 Degenerate four-wave mixing (DFWM)

The first experimental demonstration of phase conjugation by DFWM was performed by Bloom and Bjorklund (1977). In this process, a lossless nonlinear medium characterized by a third-order nonlinear susceptibility  $\chi^{(3)}$  is illuminated by two strong counterpropagating pump waves E1 and E2 and by a signal wave E3. The pump waves are usually assumed to be plane waves, although in principle any wavefront structures and amplitudes complex conjugates of one another are used. In addition, an arbitrary wavefront of the signal wave is allowed. It can interpret physically that the DFWM in the phase conjugate geometry is automatically phase-matched. Figure 1-3 shows the simple geometry for DFWM where two input beams (the forward and backward pumps) are counterpropagation. The process entails the annihilation of two pump photons and the creation of a signal and a conjugate photon. The total input energy is  $2\hbar\omega$  and the total input momentum is  $\hbar(k_1 + k_2) = 0$ , where the total output energy is  $2\hbar\omega$  and the total output momentum is  $\hbar(k_3 + k_4) = 0$ . If the two

pump beams are not exactly counterpropagation, then  $\hbar(k_1 + k_2)$  does not vanish and the phase-matched condition is not automatically satisfied [3].

One of the drawbacks of DFWM data analysis for third-order nonlinearities is that the intensity of phase conjugate wave is proportional to  $|\chi^{(3)}|^2 = |\text{Re}\{\chi^{(3)}\}|^2 + |\text{Im}\{\chi^{(3)}\}|^2$  which is attributed to TPA and optical Kerr effect both contributions. Separating the effects is difficult without performing additional experiments. Higher-order nonlinearities also can contribute, making separation of absorptive and refractive effects difficult.

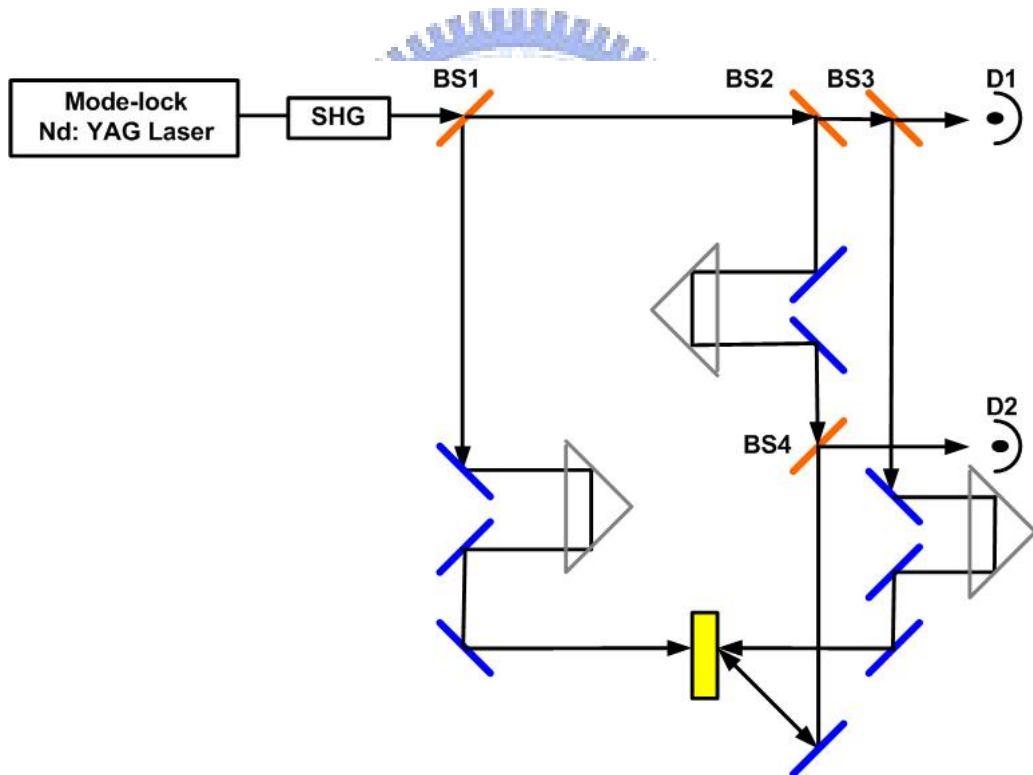


Fig. 1-3 DFWM geometry to allow temporal dynamics measurement. Detector D<sub>2</sub> monitors the conjugate beam energy.

### 1-2-2 Single beam Z-scan

Z-scan measurement was developed by Sheik-Bahae et al. in 1990 [4]. The method has

gained rapid acceptance for measuring the nonlinear refraction and absorption separately due to the simplicity of setup and interpretation. Figure 1-4 shows a standard Z-scan apparatus. The position ( $Z$ )-dependent far-field transmittance of the sample through the aperture is monitored in a photodiode. For “thin” samples (i.e.,  $L \leq n_0 Z_0$ , where  $n_0$  is the linear index), all the information is theoretically contained with a scan range of  $\pm Z_0$ . Here  $Z_0$  is the diffraction length of the focused beam defined as  $\pi w_0^2 / \lambda$  for a Gaussian beam, where  $w_0$  is the focal spot size (half-width at the  $1/e^2$  maximum in the irradiance).

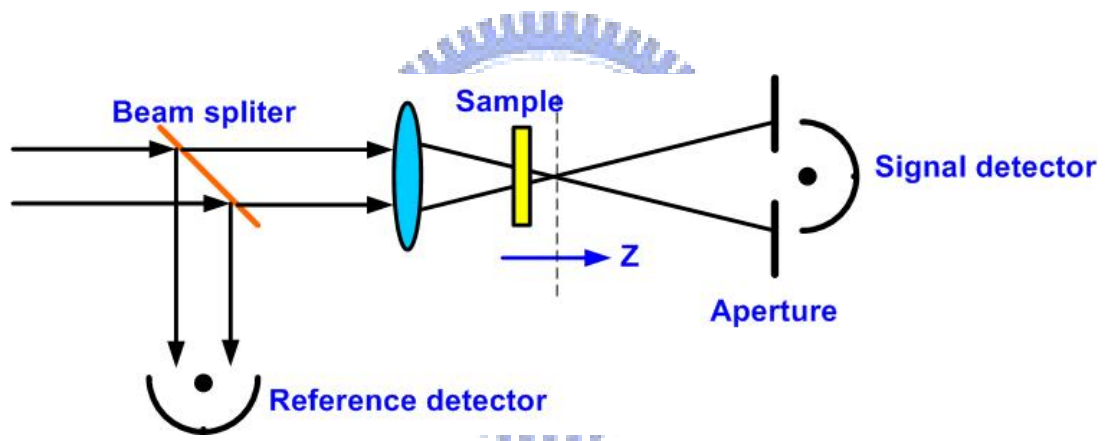


Fig. 1-4 The Z-scan experimental apparatuses in which the ratio signal/reference is recorded as a function of the sample position  $Z$ .

Figure 1-5 shows a typical Z-scan measurement for  $S=1$  that collects all the transmitted light and is insensitive to nonlinear refraction that shows a symmetric shape. Such a scheme, referred to as an “open aperture” Z-scan, is suited for measuring nonlinear absorption in the sample. The normalized transmittance shows a sharply declining in the focal point due to the maximal nonlinear absorption.

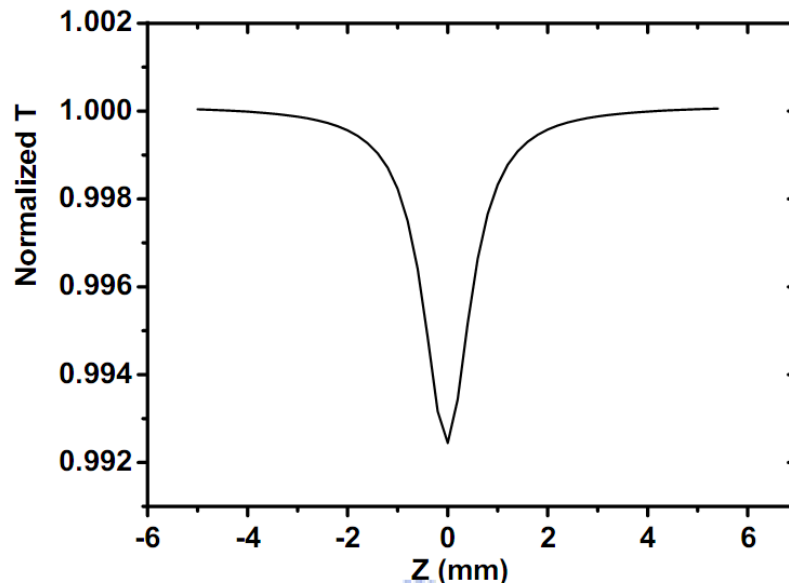


Fig. 1-5 A typical open aperture Z-scan signal for third order nonlinear absorption.

Figure 1-6 shows a typical closed aperture Z-scan due to the pure nonlinear refraction in which a self-focusing nonlinearity ( $\Delta n > 0$ ) results in a valley-peak feature in the normalized transmittance (solid line) as the sample is moved away from the lens. Before the focal position of the lens, the self-focusing results in a greater far-field divergence and a reduced aperture transmittance. While the sample placed after focus, the larger transmittance through the aperture is due to the reducing of the far-field divergence. The opposite characterization is displayed by the dash line occurring for a self-defocusing nonlinearity,  $\Delta n < 0$ . Figure 1-7 illustrates the configuration described above.

In order to obtain pure nonlinear refraction, a further division of the closed aperture Z-scan by the open aperture Z-scan data is performed. In this way, the absorptive and

refractive nonlinearities can be separated without computer fitting of the Z-scans.

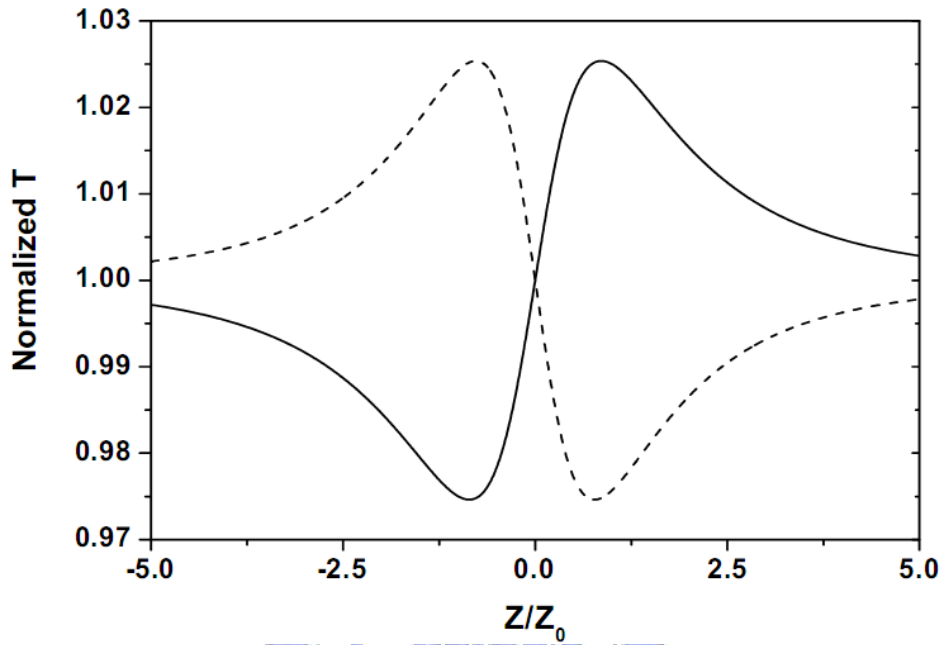


Fig. 1-6 Predicted Z-scan signal for positive (solid line) and negative (dashed line) nonlinear phase shifts.

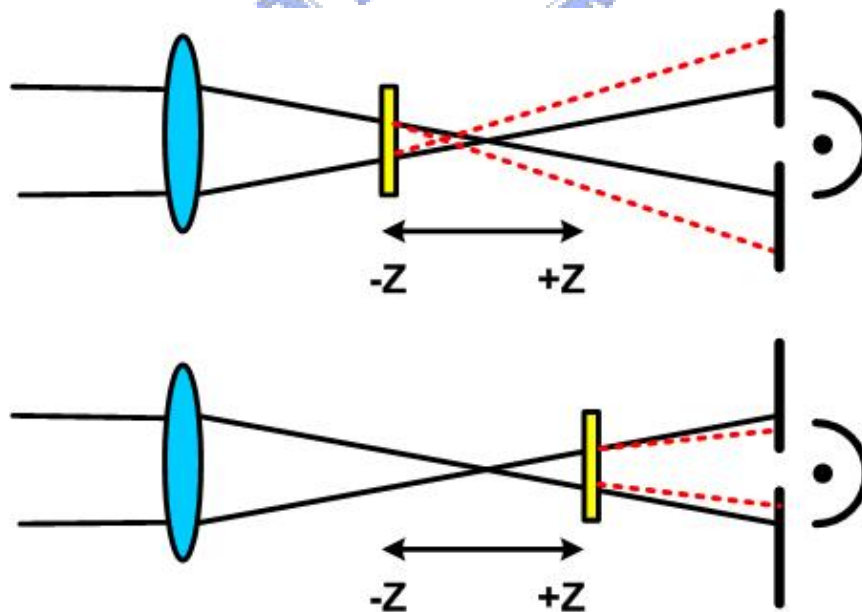


Fig. 1-7 The effect of positive self-lensing on the beam profile



## 1-3 Properties of ZnO

### 1-3-1 Merits of ZnO

ZnO is a kind of II-VI compound wide-band-gap semiconductor with a direct band gap of  $E_g = 3.37$  eV at room temperature (RT). It is a self-activated crystal of hexagonal wurtzite structure, which shown in Fig. 1-8, with lattice constant of  $a = 0.3249$  nm and  $c = 0.5207$  nm in the space group  $C_{6v}^4$ . The notable property of ZnO is due to its high exciton binding energy ( $\sim 60$  meV) that is much higher than that of ZnSe (20 meV) and GaN (27 meV). The high exciton binding energy permits excitonic recombination even at RT and can be a potential candidate for ultraviolet (UV) laser diode [5]. Besides, research on the photoluminescence (PL) properties of ZnO nanostructures has shown that, under high excitation conditions, exciton-exciton scattering as well as the recombination of electron-hole plasma is the key process leading to stimulated emission and lasing [6]. These studies demonstrated the potential of using ZnO to fabricate RT UV laser [7]. In addition to optical transparency throughout the visible region, the large piezo-optic and piezoelectric effects in films with c-axis oriented and trivalent cation-doped ZnO which exhibits marked electrical conductivity were also reported [8]. Because of these potential applications, extensive research efforts have been made on the basic physical properties of ZnO. A comprehensive review on the synthesis, mechanical, chemical, thermal and optical properties of ZnO may be found in Ref. [9].

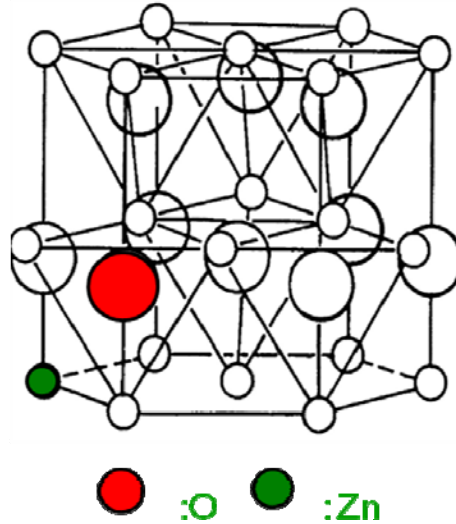


Fig. 1-8 The wurtzite structure of ZnO

### 1-3-2 Review of nonlinearity measurement of ZnO

Besides the application in UV photonic devices, the nonlinear optical properties of ZnO are also attractive. It has been shown that ZnO thin films have large nonlinear second-order optical susceptibility  $\chi^{(2)}$ , which results in efficient second-harmonic generation (SHG) [10, 11]. High conversion efficiency of the third-harmonic generation (THG) is also achieved by using an unamplified femtosecond  $\text{Cr}^{4+}$ :forsterite laser as the excitation source on a submicron-thin nanocrystalline ZnO film that was pulse-laser deposited on a fused silica substrate [12]. Moreover, the nonlinear refraction index and TPA coefficient, belong to the third order nonlinearity and can be applied in various purposes as described before, have been measured using the nanosecond and picosecond visible light [13] and femtosecond near-IR ray [14]. A TPA coefficient  $\beta$  of about 4.2 cm/GW was measured in 1mm single crystal

using 25 ps pulse at 532 nm. Especially, the studies of the TPA process in ZnO, which will lead to optical power limitation and optical damages in ZnO based optoelectronics, has been concern recently. For example, the nonlinear processes induced by TPA-excited charge carriers [15] and the multi-photon absorption (including two photon and three photon absorption) induced PL emission of ZnO under intense femtosecond excitation [16] were reported. With the different effects on photonic devices, enhancement of optical nonlinearity on ZnO was also studied in various situations such as at exciton resonance [14] and at distinct interfacial state [17].

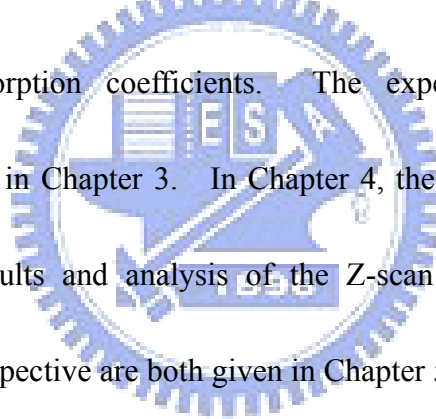
#### **1-4 Motivation**

Since ZnO shows its extensive application in the blue to UV region, it is important to study the optical properties of ZnO in its UV region instead of in IR region. However, the nonlinear properties in this regime are seldom reported. For this reason, in this thesis we focus on the optical nonlinear absorption of ZnO thin film in its below-band-gap near-UV wavelength region by using single-beam Z-scan method. Because this wavelength is in the near-resonant region, high-order nonlinearity such as free carrier absorption (FCA) was expected to occur. Besides, the enhancement of TPA due to near-exciton resonance may occur. Our previous results have observed two-photon resonance to exciton by enhancing TPA coefficient. Instead of using one-half pump photon energy, it was shown in GaN thin

film [18] that exciton could also enhance the nonlinear absorption when pump photon energy was equal to exciton transition energy. With the larger exciton binding energy of ZnO than that of GaN, we would expect observe similar resonant behaviors in ZnO thin film at RT.

## **1-5 Organization of this thesis**

In Chapter 2, we describe the background concepts and theorems of Z-scan measurements which consider both the third and fifth order nonlinearity induced by bound electronic and free carriers. We also introduce a two-band model to derive the dispersion relation of nonlinear absorption coefficients. The experimental setups for various measurements were showed in Chapter 3. In Chapter 4, the basic optical properties of the ZnO thin film and the results and analysis of the Z-scan measurements are presented. Finally, conclusions and perspective are both given in Chapter 5.



## Chapter 2 Theoretical background

### 2-1 Study of Z-scan for nonlinear absorption

Much work has been done in investigating the propagation of intense laser beams inside a nonlinear material and ensuing nonlinear refraction. In considering only a cubic nonlinearity, the index of refraction  $n$  is expressed in terms of nonlinear indexes  $n_2$  (esu) or  $\gamma$  ( $\text{m}^2/\text{W}$ ) through

$$n = n_0 + \frac{n_2}{2} |E|^2 = n_0 + \gamma I \rightarrow \Delta n(I) = \gamma I, \quad (2-1)$$

where  $n_0$  is the linear index of refraction,  $E$  is the peak electric field (cgs), and  $I$  denotes the irradiance (MKS) of the laser beam within the sample. Furthermore,  $n_2$  and  $\gamma$  are related by the conversion formula

$$n_2 \text{ (esu)} = \left( \frac{cn_0}{40\pi} \right) \gamma \text{ (m}^2/\text{W)}, \quad (2-2)$$

where  $c$  (m/s) is the speed of light in vacuum.

Assuming a TEM<sub>00</sub> Gaussian beam of beam waist  $w_0$  traveling in the  $+z$  direction and the sample length is small enough that changes in the beam diameter within the sample due to either diffraction or nonlinear refraction can be neglected, the medium is regarded as “thin”, in which case the self refraction process is referred to as “external self-action”. With above conditions and using the slowly varied envelope approximation (SVEA), a pair of simple equation is obtained:

$$\begin{cases} \frac{d\Delta\phi}{dz'} = \Delta n(I)k, \\ \frac{dI}{dz'} = -\alpha(I)I, \end{cases} \quad (2-3)$$

where  $\sqrt{I}$  is the amplitude,  $\phi$  is phase of the electric field,  $z'$  is the propagation depth in the sample and  $\alpha(I)$ , in general, includes linear and nonlinear absorption terms. In closed aperture case and only considering the linear absorption  $\alpha(I)=\alpha_0$ , Eq. (2-3) is solved to give the phase shift  $\Delta\phi$  at the exit surface of the sample which simply follows the radial variation of the incident irradiance at a given position of the sample  $z$ . Thus,

$$\Delta\phi(z, r, t) = \Delta\phi_0(z, t) \exp\left(-\frac{2r^2}{w^2(z)}\right) \quad (2-4)$$

with

$$\Delta\phi_0(z, t) = \frac{\Delta\Phi_0(t)}{1 + \frac{z^2}{z_0^2}}, \quad (2-5)$$

and  $\Delta\Phi_0(t)$ , the on-axis phase shift at the focus, is defined as

$$\Delta\Phi_0(t) = k\Delta n_0(t)L_{eff}, \quad (2-6)$$

where  $w^2 = w_0^2(1 + z^2/z_0^2)$  is the beam radius,  $R(z) = z(1 + z_0^2/z^2)$  is the radius of curvature of the wavefront at  $z$ ,  $z_0 = kw_0^2/2$  is the diffraction length of the beam,  $k = 2\pi/\lambda$  is the wave vector,  $\lambda$  is the laser wavelength,  $L_{eff} = (1 - e^{-\alpha_0 L})/\alpha_0$ , with  $L$  the sample length and  $\alpha_0$  the linear absorption coefficient. The complex electric field exiting the sample  $E_e$  now contains the nonlinear phase distortion

$$E_e(r, z, t) = E(r, z, t) e^{-\alpha_0 L/2} e^{i\Delta\phi(z, r, t)}, \quad (2-7)$$

where  $E(r, z, t)$  is the electric field of incident into sample. By using Huygen's principle, one

can obtain the far-field pattern of the beam at the aperture plane through a zeroth-order Hankel transformation of  $E_e$ . Here, a more convenient treatment applicable to Gaussian input beam which is referred to as the ‘‘Gaussian decomposition’’ (GD) method is used. In which the complex electric field at the exit plane of the sample is decomposed into a summation of Gaussian beams through a Taylor series expansion of the nonlinear phase term  $e^{i\Delta\phi(z,r,t)}$  in Eq. (2-7). That is,

$$e^{i\Delta\phi(z,r,t)} = \sum_{m=0}^{\infty} \frac{[i\Delta\phi_0(z,t)]^m}{m!} e^{-2mr^2/w^2(z)} \quad (2-8)$$

Each Gaussian beam can be simply propagated to the aperture plane where they will be resumed to reconstruct the beam and resulted in a compound electric field of  $E_a(z,r,t)$ . The transmitted power through the aperture is obtained by spatially integrating  $E_a(z,r,t)$  up to the aperture radius  $r_a$ , giving

$$P_T(\Delta\Phi_0(t)) = c\varepsilon_0 n_0 \pi \int_0^{r_a} |E_a(z,r,t)|^2 r dr, \quad (2-9)$$

where  $\varepsilon_0$  is the permittivity of vacuum. Including the pulse temporal variation, the normalized Z-scan transmittance  $T(z)$  can be calculated as

$$T(z) = \frac{\int_{-\infty}^{\infty} P_T(\Delta\Phi_0(t)) dt}{S \int_{-\infty}^{\infty} P_i(t) dt}, \quad (2-10)$$

where  $P_i(t) = \pi w_0^2 I_0(t)/2$  is the instantaneous input power and  $S = 1 - e^{-2r_a^2/w_a^2}$  is the aperture linear transmittance, with  $w_a$  denoting the beam radius at the aperture in the linear regime. If

the nonlinearity is cubic, small phase change and  $d \gg z_0$  (far-field condition), the on-axis electric field at the aperture plane can be obtained by letting  $r = 0$ . Following such simplifications, the normalized Z-scan transmittance can be written as

$$T(z, \Delta\Phi_0) = \frac{|E_a(r=0, z, \Delta\phi_0)|^2}{|E_a(r=0, z, \Delta\phi_0=0)|^2} \cong 1 + \frac{4x}{(x^2+9)(x^2+1)} \Delta\Phi_0, \quad (2-11)$$

where  $x=z/z_0$ . Eq. (2-11) is the fitting formula for nonlinearity due to nonlinear refraction.

Next, considering the nonlinear absorption such as two photon absorption (TPA), Eq. (2-3) will be reexamined after the substitution:

$$\alpha(I) = \alpha_0 + \beta_0 I, \quad (2-12)$$

where  $\beta_0$  is the TPA coefficient. Following the same procedures, the total transmitted fluence in the case of open aperture can be shown as follows:

$$P(z, t) = P_i(t) e^{-\alpha z} \frac{\ln[1+q_0(z, t)]}{q_0(z, t)}, \quad (2-13)$$

where  $q_0 = \frac{\beta_0 I_0(t) L_{eff}}{(1 + \frac{z^2}{z_0^2})}$  and  $P_i(t) = \frac{\pi w_0^2 I_0(t)}{2}$ . For a temporally Gaussian pulse, Eq. (2-13)

can be time integrated to give the normalized energy transmittance

$$T(z, S=1) = \frac{1}{\sqrt{\pi} q_0(z, 0)} \int_{-\infty}^{\infty} \ln[1+q_0(z, 0) e^{-\tau^2}] d\tau. \quad (2-14)$$

For  $|q_0| < 1$ , this transmittance can be expressed in terms of the peak irradiance in a summation form more suitable for numerical evaluation:

$$T(z, S=1) = \sum_{m=0}^{\infty} \frac{[-q_0(z, 0)]^m}{(m+1)^{3/2}}. \quad (2-15)$$

Eq. (2-14) is the fitting formula for nonlinearity resulted from two photon absorption.



At higher irradiance level the nonlinear refraction caused by TPA-generated free charge carriers, an effective fifth-order nonlinearity becomes significant. Thus the change of refractive index will become:

$$\Delta n \cong \gamma I_0 + C \sigma_r I_0^2, \quad (2-16)$$

where  $C = 0.23(\beta_0 t_0 / \hbar \omega)$  for low linear absorption ( $\alpha_0 L < 0.2$ ),  $t_0$  is the pulse width. The analytic procedures which involved free carriers are the same as the above descriptions.

## 2-2 Modified model for high-order nonlinearities

In Section 2-1, we introduce the mathematical theory of Z-scan measurement which only considers a cubic nonlinearity. However, at the higher excitation irradiance, the nonlinear effects originating from the two-photon-excited free carriers proved to be more significant [19]. Similar to nonlinear refraction, the two-photon-excited free carriers would also function as an effective fifth-order nonlinearity on nonlinear absorption. As a result, when a TEM<sub>00</sub> Gaussian beam propagates in a thin sample with a physical length  $L$ , the optical loss now can be described by

$$\frac{dI}{dz'} = -(\alpha + \beta_0 I + \sigma_a N)I, \quad (2-17)$$

where  $\sigma_a$  is the carrier absorption cross-section, and  $N$  is the carrier density. The photo-generated carrier concentration is governed by

$$\frac{dN}{dt} = \frac{\alpha_0 I}{\hbar \omega} + \frac{\beta_0 I^2}{2\hbar \omega}. \quad (2-18)$$

Eq. (2-18) includes both one-photon and two-photon-excited carrier generation, because in our measurements, the excitation wavelength (390-420 nm) is near the absorption edge of ZnO, therefore the contribution of linear absorption to free carrier generation should be considered [20]. Thus, the first and the second terms in Eq. (2-18) indicate the creation of one electron-hole pair for every one absorbed photon and two absorbed photons, respectively.

To simplify these equations, we use

$$N \cong \frac{\alpha_0 I}{\hbar\omega} \tau_a + \frac{\beta_0 I^2}{2\hbar\omega} \tau_a, \quad (2-19)$$

where  $\tau_a$  is the lifetime of free carrier. When the pulse duration of laser  $\tau_p$  is shorter than the lifetime of free carrier,  $\tau_a$  should be replaced with  $\tau_p$ . Hence, Eq. (2-18) can be rewritten as

$$\frac{dI}{dz'} = -\alpha_0 I - \beta I^2 + DI^3. \quad (2-20)$$

Notice that now the effective third-order nonlinearity  $\beta = \beta_0 + \frac{\sigma_a \alpha_0 \tau_p}{\hbar\omega}$

contains the contribution of TPA and carrier generated by linear absorption, and the effective

fifth-order nonlinearity  $D = \frac{\sigma_a \beta_0 \tau_p}{2\hbar\omega}$ , which presents the contribution of carrier generated by

TPA. By solving Eq. (2-20) and then integrating it over the spatially and temporally by

highly efficient Simpson arithmetic, we can obtain an analytic expression as follows [21]:

$$T(z) = \frac{\ln(1+q')}{q'} \frac{\ln[(1+p'^2)^{1/2} + p']}{p'} f(q', p'), \quad (2-21)$$

where

$$f(p', q') = \frac{\sum_{n=0}^5 a_n p'^n + q' \sum_{n=0}^5 b_n p'^n}{1 + q' \sum_{n=0}^5 c_n p'^n}, \quad (2-22)$$

$q'$  and  $p'$  are given by  $q' = q'_0 / (1 + \frac{z^2}{z_0^2})$  and  $p' = p'_0 / (1 + \frac{z^2}{z_0^2})$ , respectively, with  $q'_0 = \beta I_0 L_{eff}$  and  $p'_0 = (2DI_0^2 L'_{eff})^{1/2}$  being the on-axis peak phase shifts caused by the third and fifth-order nonlinear absorption processes, respectively. Here,  $I_0$  is the on-axis peak intensity at the waist, and  $L'_{eff} = [1 - e^{-2\alpha_0 L}] / 2\alpha_0$ ,  $z_0$  and  $L_{eff}$  are Rayleigh length and effective length defined in Section 2-1. When considering the temporal profile as Gaussian or hyperbolic secant (sech) of the spatial Gaussian laser pulses, the coefficients  $a_n$ ,  $b_n$ , and  $c_n$  in Eq. (2-22) are listed in Table I. It has been confirmed that all the empirical formulae have an error of 0.5% at the utmost with respect to the exact numerical results when  $0 \leq q'_0 \leq \pi$  and  $0 \leq p'_0 \leq \pi$ . For the pure TPA ( $D = 0$ ) and 3PA ( $\beta = 0$ ), Eq. (2-21) degenerates into the following forms, respectively:

$$T(z) = \frac{(a_0 + b_0 q') \ln(1 + q')}{q'(1 + c_0 q')}, \quad (2-23a)$$

$$T(z) = \ln[(1 + p'^2)^{1/2} + p'] \sum_{n=0}^5 a_n p'^{n-1}. \quad (2-23b)$$

Of course, Eq. (2-21) can also be used to describe the intensity-dependent nonlinear transmission. Setting  $z = 0$  in Eq. (2-21), we yield  $T(0)$  as a function of  $I_0$ ,

$$T(0) = \frac{\ln(1 + q'_0)}{q'_0} \frac{\ln[(1 + p_0'^2)^{1/2} + p'_0]}{p'_0} f'_0, \quad (2-24)$$

where  $f'_0 = f(q'_0, p'_0)$ . Eq. (2-24) is also the fitting equation we used in our experiments.

Table I Coefficients  $a_n$ ,  $b_n$ , and  $c_n$  for temporal Gaussian and sech pulses when  $0 \leq q'_0 \leq \pi$  and  $0 \leq p'_0 \leq \pi$ .

n	Gaussian			Sech		
	$a_n$	$b_n$	$c_n$	$a_n$	$b_n$	$c_n$
0	1.000	0.4364	0.3036	1.000	0.4254	0.2744
1	-0.0067	0.0002	0.0268	-0.0053	0.0077	0.0158
2	0.1002	0.4143	0.1961	0.1063	0.3619	0.1615
3	-0.0550	-0.3080	-0.1946	-0.055	-0.2516	-0.1511
4	0.0136	0.0882	0.0636	0.0131	0.0690	0.0477
5	-0.0013	-0.0091	-0.0071	-0.0012	-0.0069	-0.0052

### 2-3 Dispersion of nonlinear absorption

Here a two-band model is used to calculate the scaling and spectrum of the nondegenerate nonlinear absorption  $\Delta\alpha(\omega_1, \omega_2)$ . The model includes the ac Stark shift, the electronic Raman effect and TPA. For nonlinear absorption, the second order perturbation theory is used here to deal with TPA processes.

In the beginning, the electric dipole approximation for the radiation interaction Hamiltonian is taken and then the transition rate will be calculated using an S-matrix formalism [22]

$$S = \frac{i\pi}{\hbar} \frac{e\hat{a} \cdot p_{vc}}{m_0 c} \sum_{m,n=-\infty}^{\infty} J_m(\eta_1) J_n(\eta_2) \cdot \{A_{01}[\delta((m+1)\omega_1 + n\omega_2 + \omega_{vc}) + \delta((m-1)\omega_1 + n\omega_2 + \omega_{vc})] + A_{02}[\delta(m\omega_1 + (n+1)\omega_2 + \omega_{vc}) + \delta(m\omega_1 + (n-1)\omega_2 + \omega_{vc})]\}. \quad (2-25)$$

From the S-matrix description, the transition rate can be determined to define the absorption

coefficient. The resultant expression for a change of absorption in nondegenerate case using the second-order perturbation approach is

$$\Delta\alpha(\omega_1, \omega_2) = 2K \frac{\sqrt{E_p}}{n_1 n_2 E_g^3} F_2\left(\frac{\hbar\omega_1}{E_g}, \frac{\hbar\omega_2}{E_g}\right) I_2. \quad (2-26)$$

The function  $F_2$  is a function of the ratio of the photon energy  $\hbar\omega$  to  $E_g$  (i.e., denoting the optically coupled states). The different form of the functional  $F_2$  depends on the assigning band structure and the intermediate states.  $E_p$  is nearly material independent and possesses a value  $E_p \approx 21$  eV for most direct band gap semiconductors, and  $K$  is a material-independent constant that is defined as

$$K = \frac{2^9 \pi e^4}{5 \sqrt{m_0 c^2}}. \quad (2-27)$$

The value of  $K$  is 1940 whose units depend on  $\beta$  in  $cm/GW$ , and  $E_g$  and  $E_p$  in eV.

The absorption spectral function  $F_2(x_1, x_2)$  is resulted from TPA, Raman and ac Stark effect that is presented in Table II. In Raman transition, an electron is excited from the valence band into the conduction band via absorption of a photon at  $\hbar\omega_1$  and emission a photon at  $\hbar\omega_2$  ( $\omega_1 > \omega_2$ , Stoke) and vice versa ( $\omega_1 < \omega_2$ , anti-Stoke). The TPA occurs when the sum of the frequencies is equal to the band gap. However, the Raman term turns on when the difference of the frequencies is equal to the band gap so that one frequency must exceed the band gap. Absorption coefficient can also be changed due to a shift in band gap as a result of the ac Stark effect. For example, a change in the linear absorption of the light

with the frequency  $\omega_1$  occurs when the bands are shift due to the ac Stark effect caused by the exciting light with frequency  $\omega_2$  near band-edge. Two different kinds of ac Stark effect can be occurred. If the transition of  $\omega_1$  is the conduction (or valence) band to itself, is termed the linear Stark effect. Otherwise, the transition from the conduction band to the valence band, it is termed the quadratic Stark effect. The same condition can be generated in the ac Stark effect depending on  $\hbar\omega_1 > E_g$  or  $\hbar\omega_2 > E_g$ .

Table II Contributions to the nonlinear absorption spectral function  $F_2(x_1, x_2)$

Contribution	$F_2(x_1, x_2)$
<b>Two photon absorption</b> $(x_1+x_2>1)$	$\frac{(x_1+x_2-1)^{3/2}}{2^7 x_1 x_2^2} \left(\frac{1}{x_1} + \frac{1}{x_2}\right)^2$
<b>Raman</b> $(x_1-x_2>1)$	$\frac{(x_1-x_2-1)^{3/2}}{2^7 x_1 x_2^2} \left(\frac{1}{x_1} - \frac{1}{x_2}\right)^2$
<b>AC Stark</b> $(x_1>1)$	$-\frac{1}{2^9 x_1 x_2^2 (x_1-1)^{1/2}} \left[ \frac{x_1}{x_1^2 - x_2^2} - \frac{2(x_1-1)(x_1^2 + x_2^2)}{(x_1^2 - x_2^2)^2} + \frac{8(x_1-1)^2}{x_2^2} \right]$

## Chapter 3 Experiments

Our high-quality 4.3- $\mu\text{m}$ -thick ZnO film was grown on a fused silica substrate by laser MBE. The experimental setups for various measurements will be described in this chapter.

### 3-1 Measurement of basic characteristics

#### 3-1-1 Photoluminescence detection system

A UV He-Cd laser (Kimmon IK5552R-F) operating at wavelength 325 nm is utilized as the pumping source for photoluminescence (PL). Figure 3-1 shows the block diagram of PL detection system, it includes the reflective mirror, focusing and collecting lenses, and the single-grating monochromators (TRIAX 320) with a photo-multiplier tube (PMT-HVPS) which is equipped with a photon counter. The TRIAX 320 monochromator has three selectable resolutions of lines 600, 1200 and 1800 grooves/mm. The normal applied voltage of PMT is 0.8 KV. We used standard fluorescent lamps to calibrate our spectral response of spectrometer and detection system. The signals of PL spectra are exposed about 0.1sec at each step of 0.1 nm. When the entrance and exit slits are both opened about 50  $\mu\text{m}$ , the resolution is about 0.1 nm in the system.

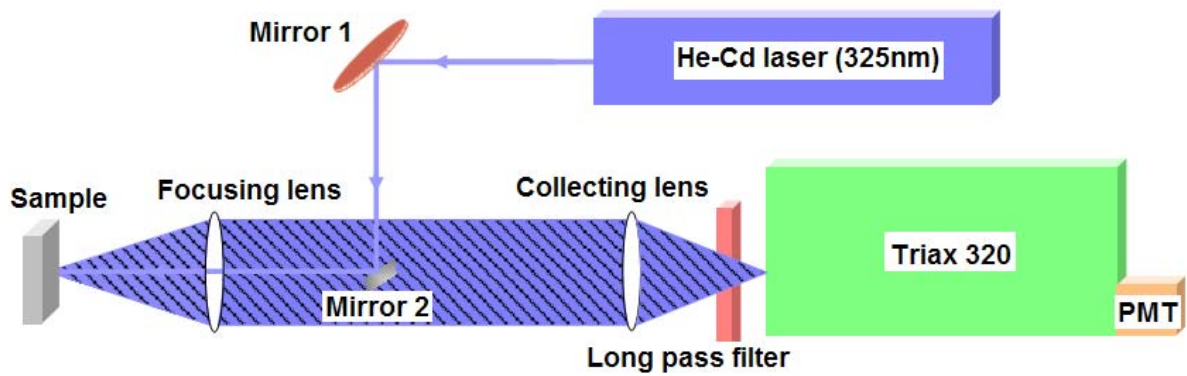


Fig. 3-1 Sketch diagram of photoluminescence spectrum.

### 3-1-2 Transmittance and absorbance detection system

The transmittance and reflectance spectra were measured using a Lambda 950 spectrophotometer (Perkin Elmer Inc). The spectrophotometer uses a gridless PMT with Peltier-controlled PbS detector to achieve high-performance testing across the spectral range from 175 nm to 3300 nm. The UV and VIS resolution can reach 0.05 nm, while the NIR resolution reaches up to 0.20 nm. In our experiments, we scanned the wavelength from 300 nm to 800 nm and set a resolution of 1 nm.



## **3-2 Experimental system of single beam Z-scan**

### **3-2-1 Light source system**

A commercial Kerr-lens mode-locked Ti:sapphire laser (Spectra-Physics inc., Tsunami) is used as the near-IR light source which is pumped by a diode-pump solid state laser (Spectra-Physics inc., Millennia) that is a CW laser with a wavelength of 532 nm and maximum power of about 10 W. In our measurements, we chose 8.5 W to take as the pump power. The structure of Ti:sapphire laser is shown in Fig. 3-2. The output wavelength is tunable from 690-1080 nm using a prism sequence and a slit inside the laser cavity with a repetition rate of 82MHz. Power of the output laser beam we used is about 1-1.5 W.

For short wavelength, a frequency doubler (Spectra-physics No. 3980), in which a BBO (barium beta borate) is taken as SHG (second harmonic generation) crystal, is also used to convert the near-IR wavelength into near-UV wavelength. The output power from the doubler is about 200 mW.

### **3-2-2 Z-scan implement**

The apparatus of single beam Z-scan is shown in Fig. 3-3. We use a commercial ultrafast Ti:sapphire laser with doubled-frequency described in the last section as the exciting source. The operating wavelength was tuned between 390 nm and 420 nm. The laser has nearly Gaussian spatial mode distribution and the full width at half maximum pulsewidth

around 200 fs. The femtosecond near-UV pulses provide a large peak intensity to induce third-order or fifth-order nonlinearity in ZnO.

The incident light is chopped by a chopper with 2 kHz frequency and divided into two beams by a beam splitter. The reflected beam was detected by a photodiode as the reference light. The transmitted beam, as the exciting light, was focused into the sample by an objective lens with a focal-length of 17-19 mm due to different pump wavelength and the focused beam radius  $w_0$  is around 3.5  $\mu\text{m}$ -5  $\mu\text{m}$  at the focus point, which varied with wavelength. Our sample was mounted on a step-motor with a resolution of 0.1  $\mu\text{m}$  movement per step for precise moving along the Z-axis. The transmitting light through the sample was detected by another photodiode as the signal. The electric signals from the two photodiodes were connected to a lock-in amplifier (Stanford Research SR830) to enhance the signal-to-noise ratio. The aperture was opened completely to obtain the open aperture z-scan trace ( $S = 1$ ) which implies nonlinear absorption. An irradiance-dependent Z-scan study will be performed to investigate the behavior of free carrier absorption (FCA), an effective fifth-order nonlinearity, in which the free carriers were generated by TPA. A wavelength-dependent Z-scan will be also presented for the resonance behaviors.

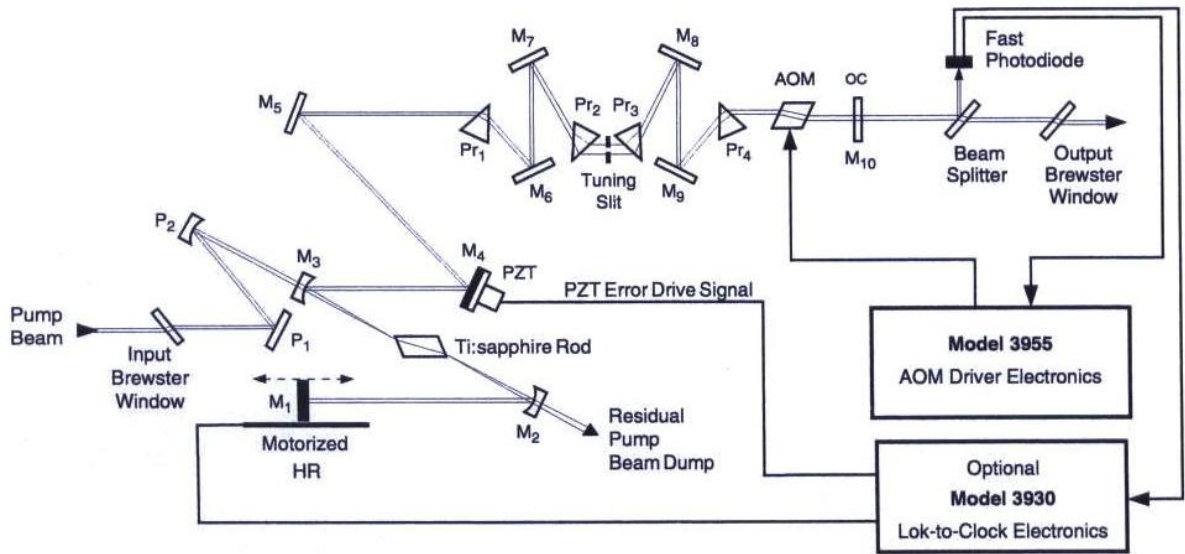


Fig. 3-2 The optical beam path for Tsunami mode 3960C femtosecond configuration.

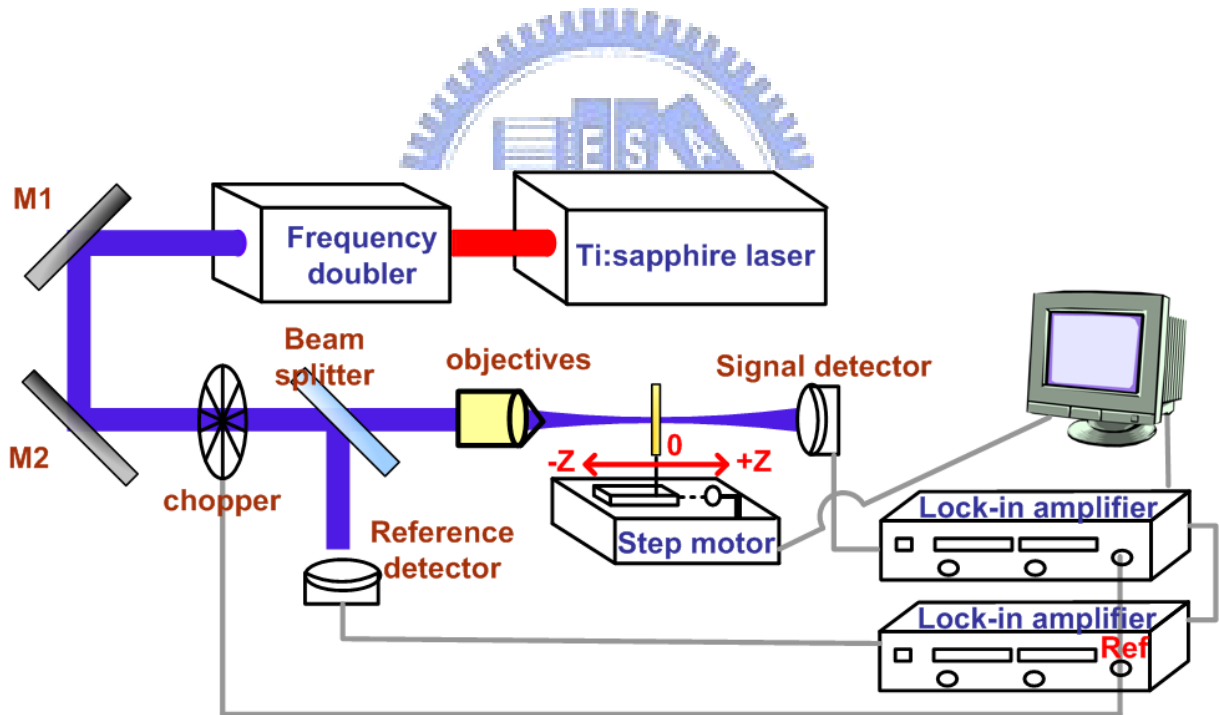


Fig. 3-3 The Z-scan apparatus with reference detector and lock-in amplifier to minimize background and maximize the signal-to-noise ratio respectively.

## Chapter 4 Results and Discussion

### 4-1 Basic properties of ZnO thin films

Before investigating the nonlinear optical properties, we need to know the basic properties of our samples first to give some provident information for further nonlinear optical study. We would show the photoluminescence spectrum, x-ray diffraction pattern, and transmission and reflection spectra in the succeeding three sections.

#### 4-1-1 Photoluminescence spectrum

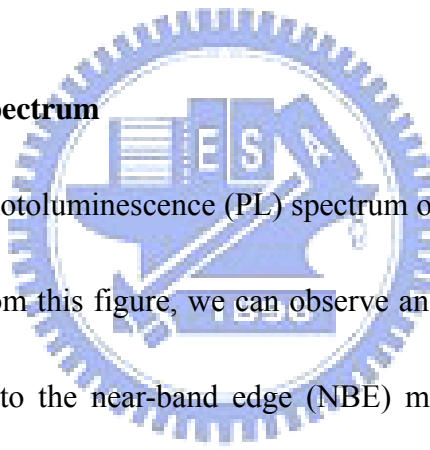


Figure 4-1 shows the photoluminescence (PL) spectrum of ZnO thin film at an excitation wavelength of 325 nm. From this figure, we can observe an obvious emission band around 380 nm, which is assigned to the near-band edge (NBE) mission due to an exciton state, because the exciton binding energy is around 60 meV. The main features of PL spectra at room temperature are similar for most of the epitaxial ZnO samples. The inset, which is the magnified segment of 450 nm-600 nm, shows another weak broadband emission in the green region. This broad band emission is contributed from the defect or the surface state emission that is due to lattice mismatch of fused silica and ZnO.

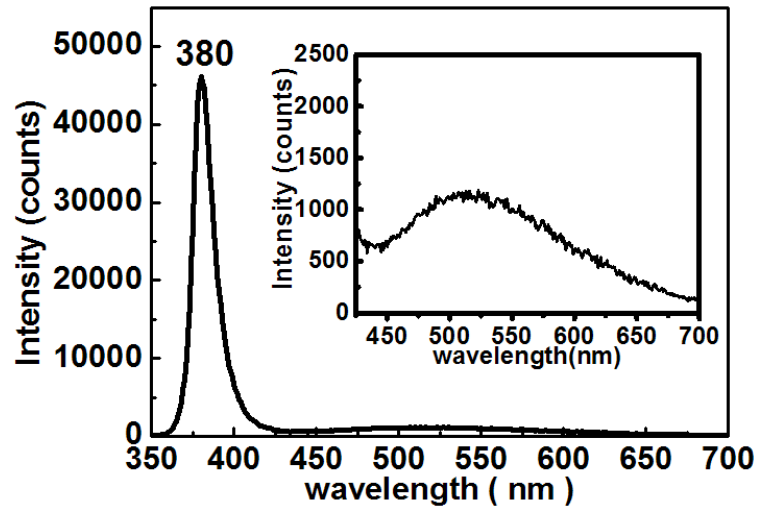


Fig. 4-1 Fluorescence spectrum of ZnO thin film

#### 4-1-2 X-ray diffraction

The crystal structure of our ZnO thin film were inspected by a X-ray diffractometer with a  $\text{CuK}\alpha$  line ( $1.5405 \text{ \AA}$ ) and a typical X-ray diffraction pattern is shown in Fig. 4-2. By comparing with JCPDS#36-145 and our diffraction pattern, a strong diffraction line was only observed from the (002) plane. This result indicates that the ZnO sample is single crystalline thin film with the crystallographic c-axis being parallel to the growth direction or perpendicular to the surface of this sample.

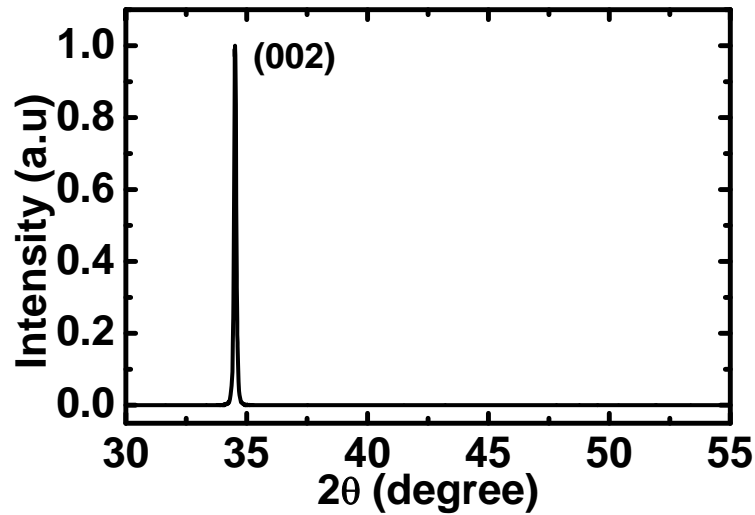


Fig. 4-2 X-ray diffraction pattern of ZnO thin film

#### 4-1-3 Transmission and reflection spectra

Figure 4-3 illustrates the transmission and reflection spectra of our ZnO thin film. Both of the figures show obvious interference fringes in which we can acquire the information of thickness and linear absorption coefficient. The extra peak in the reflection spectrum corresponds to the exciton resonance, which is coincidence with PL spectral peak in Fig. 4-1.

To acquire thickness of ZnO thin film, we apply the formula [23]:

$$L = \frac{M\lambda_1\lambda_2}{2[n(\lambda_1)\lambda_2 - n(\lambda_2)\lambda_1]},$$

where L is the thickness of the sample, M is the number of oscillations between two extrema (M=1 between two consecutive maxima or minima), and  $\lambda_1, n(\lambda_1), \lambda_2, n(\lambda_2)$  are the corresponding wavelengths and indices of refraction. And the formulas [23]:

$$n = [N + (N^2 - n_0^2 n_1^2)^{1/2}]^{1/2},$$

$$N = \frac{n_0^2 + n_1^2}{2} + 2n_0 n_1 \frac{T_{\max} - T_{\min}}{T_{\max} T_{\min}},$$

where  $n_0$  and  $n_1$  are the refractive indices of air and substrate, respectively. By taking  $n_0=1$ ,  $n_1=1.5$ ,  $\lambda_1=542$  nm, and  $\lambda_2=566$  nm, we can evaluate thickness of our sample is about 4.3 $\mu$ m.

Knowing the thickness, we also can calculate the linear absorption coefficient by using  $T = (1 - R)^2 \exp(-\alpha L)$ , where T is the transmittance, R is the reflectance, and  $\alpha$  is linear absorption coefficient. Using  $L = 4.3 \mu\text{m}$ , we obtain  $\alpha = 5147\text{cm}^{-1} \sim 7338\text{cm}^{-1}$  for wavelength of 420 nm ~390 nm.

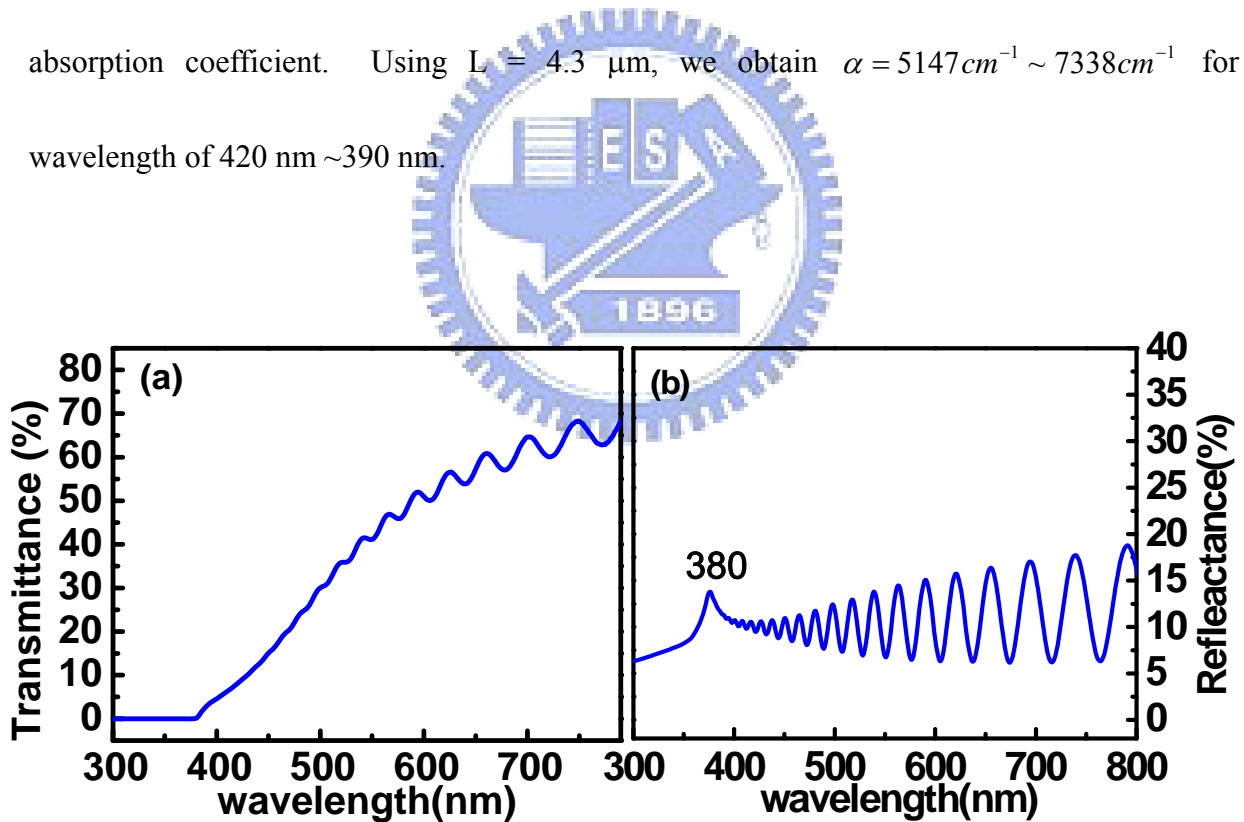


Fig. 4-3 The optical transmittance and reflectance spectra of the ZnO thin film

## 4-2 Z-scan measurement in near-resonant regime

### 4-2-1 Nonlinear absorption of ZnO thin film

In order to investigate the nonlinear absorption of ZnO at blue wavelengths, we performed a series of open aperture Z-scan with pumping wavelength close to the band gap of ZnO, which was measured in the near-resonant region. Figure 4-4 shows the typical Z-scan curves under different input irradiances at 400 nm. Herein the input irradiance is defined as the maximum irradiance at the focal point on the Z axis. The symbols are experimental data while the solid lines are the theoretically fitting curves by using Eq. (2-15). The symmetric valley relative to the focal point ( $z = 0$ ) shows an obvious nonlinear absorption and the nonlinear signals increased seriously as the peak irradiance increased. In order to make sure this signals were not contributed from the quartz substrate, we also repeated our measurement on a comparison quartz substrate, and no signal was found.

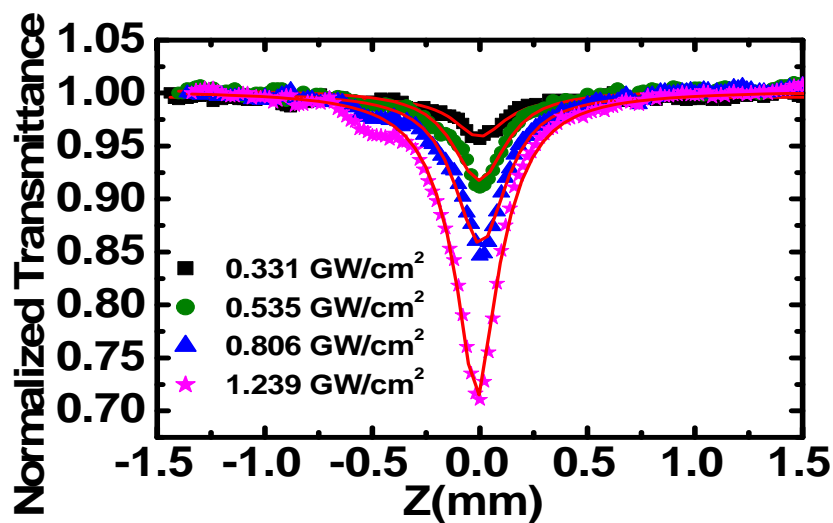


Fig. 4-4 Open aperture Z-scan traces of ZnO thin film at 400 nm. The symbols are experimental data and the solid lines are theoretically fitting curves by theory.



As known, nonlinear optical response of semiconductor arises from a variety of physical mechanisms based on parameters such as the wavelength, pulse duration and intensity of the excited radiation, and the processes involved in nonlinear absorption are generally multiphoton absorption, dynamic free carrier absorption (FCA), and saturation of single photon absorption, etc. Therefore the z-scan profile of open-aperture could have either a central valley or a central peak. With the results shown in Fig 4-4, the possibility of saturation of linear absorption has been excluded. To further investigate the mechanism, we inspected the relation between nonlinear absorption and input intensity. Figure 4-5 shows the dependence of parameter  $q_0$  and input irradiance  $I_0$  in logarithm scale. The parameter  $q_0$  is the depth of the open aperture Z-scan curve obtained from theoretically fitting utilizing Eq. (2-15). Through the equation  $q_0 = \beta_{eff} I_0 L_{eff}$ , where  $\beta_{eff}$  now replaces  $\beta_0$  and represents the effective two photon absorption (TPA) coefficient and  $I_0$  is the input intensity, we know that if TPA process is the only mechanism of nonlinear absorption, the slope of logarithm  $q$  versus logarithm  $I_0$  would be equivalent to one. However, the slope is equal to 1.6, which is larger than one. For this reason, besides TPA is the basic mechanism, there is the possibility of higher order nonlinear processes such as FCA contributing to the induced absorption in our samples.

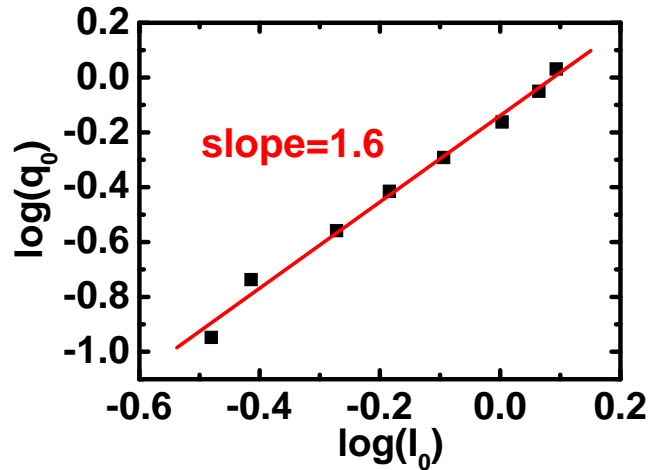


Fig. 4-5 Variation of  $\log q$  as a function of  $\log I_0$  for ZnO thin film at a wavelength of 400 nm.

Here we introduce the process used to obtain the effective two photon absorption coefficient  $\beta_{eff}$ . The two-photon absorption model developed by Shiek-Bahae et al. [4] which had been described in Section 2-1, is the most general method to acquire two photon absorption coefficient. However, Eq. (2-15) is only suitable for  $|q_0| < 1$ , where  $q_0$  is equivalent to the strength of nonlinear absorption. In our situation, when the pump wavelength was close to band gap energy, the nonlinear absorption was too strong to guarantee  $|q_0| < 1$ , especially at the wavelength of 390 nm. Therefore, we use another modified model that considers higher nonlinear absorption [21] and utilizes Eq. (2-23a) to fit Z-scan traces in Fig. 4-6, which presents the open aperture Z-scan traces of ZnO thin film at 390 nm. Table III is the comparison of the fitting results by using two different equations mentioned above. We observed the Rayleigh range will become irradiance-dependent if Eq. (2-15) was used as fitting equation, and the related beam waist through  $z_0 = \pi\omega_0^2 / \lambda$  won't be

a constant either. Using the result to infer the peak irradiance would lead to large errors in the calculation of nonlinear parameters.

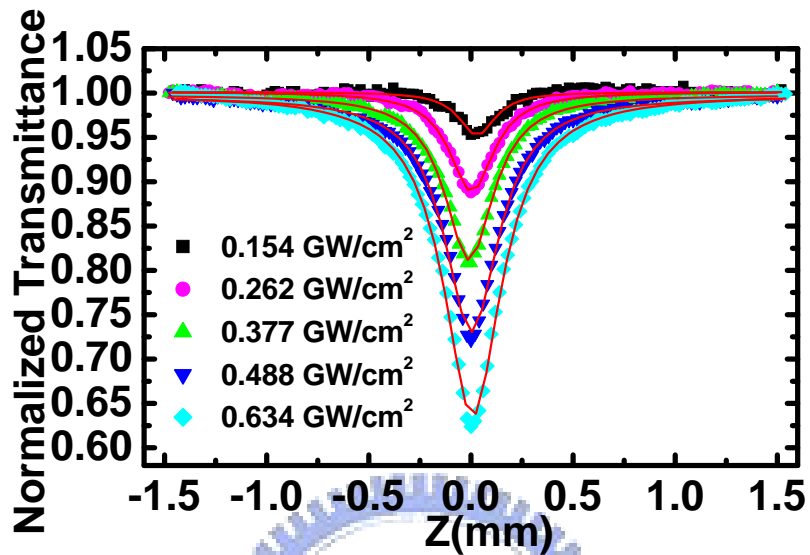


Fig. 4-6 Open aperture Z-scan traces of ZnO thin film at 390 nm. The symbols are experimental data and the solid lines are theoretically fitting curves by modified theory.

Table III. Comparison of the fitted results for Z-scan traces by fitting equations of SB model and high-order model respectively.

Power (mW)	High-order model (our fitting equation)[21]		Shiek-Bahae model (SB)[4]	
	Rayleigh length $z_0$ (mm)	Beam waist $w_0$ (mm)	Rayleigh length $z_0$ (mm)	Beam waist $w_0$ (mm)
1	0.102	3.550	0.102	3.556
2	0.119	3.851	0.120	3.867
3	0.124	3.929	0.128	3.988
4	0.128	3.988	0.148	4.287
5	0.123	3.912	0.185	4.786
6	0.114	3.766	0.226	5.291

Figure 4-7 displays the fitted values of  $\beta_{eff}$  at 390 nm as a function of input intensity when using two different models. Evident errors in the calculation of two photon absorption especially under high intensity were shown in circle symbols, the results indicated the modified model should be used in our measurements. Instead of a constant value in the near-IR region [14],  $\beta_{eff}$  increased linearly following the input intensity, suggesting that the sample should exhibit FCA other than TPA as the pump wavelength near the band-edge. FCA could be treated as an effective fifth-order (sequential  $\chi^{(3)}:\chi^{(2)}$  effect) nonlinearity arising from TPA-generated carriers. Such a TPA assisted excited state absorption has been previously reported for Au nanoparticles using 7 ns pulse duration excitation at 532 nm [24]. It was reported that the high order nonlinearities based on the free carriers are expected under the following conditions: (1) the laser pulse width is close to the lifetime of free carrier; [25, 26] (2) the input intensity is high enough; [27] (3) the pump wavelength is near to the band gap of the sample. In condition (1), because the order of laser pulse width and lifetime of free carrier is similar, the trailing edge of the pulse will result in further absorption of two-photon-excited free carriers generated by the leading edge of the pulse. In conditions (2) and (3), a large number of free carriers would be generated by TPA, so the possibility of FCA becomes strong. Although the lifetime of free carrier in ZnO is 2.8 ns [13], which is longer than our femtosecond pulse, the used excitation wavelength is very close to the band gap energy of ZnO. Hence, the effect of free carrier can't be ignored. Besides,  $\beta$ , which is

mainly contributed from intrinsic TPA of ZnO , was also obtained from the intercept of the fitted line with the vertical axis in Fig. 4-7, which was equal to 1632 GW/cm<sup>2</sup>.

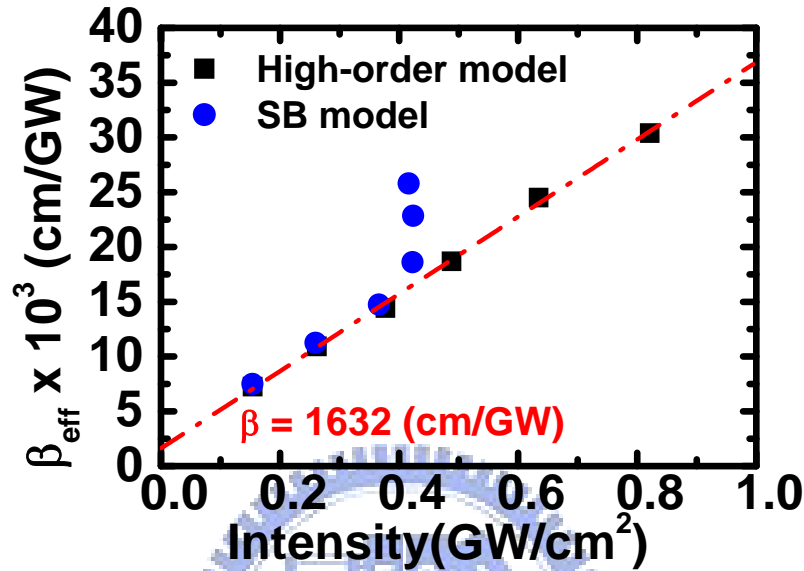


Fig. 4-7 Comparison of the variation in effective TPA coefficient with the input intensity at pump wavelength of 390 nm. The black square and blue circle are the results by two different fitting methods. The intercept of fitting straight line gives  $\beta = 1632(\text{cm}/\text{GW})$ , which mainly contributed from intrinsic TPA of ZnO.

We also performed Z-scan measurement at the longer wavelength. Figure 4-8 shows the comparison of open aperture Z-scan measurements under different intensity at 420 nm. Note that a peak instead of a dip under the lower intensity was observed. This phenomenon was attributed to saturation of the linear absorption due to ZnO defect states that could be proved in Fig. 4-9. Figure 4-9 is a plot of  $(\alpha h\nu)^2$  versus energy acquired from the relation:  $\alpha h\nu = A(h\nu - E_g)^{1/2}$  [28], where  $\alpha$  is the absorption coefficient derived in Section 4-1-3,  $A$  is an energy-independent constant,  $E_g$  is the band gap energy, and  $h\nu$  is the energy of incident light. From the intercept on the energy by extrapolating the linear part of the curve

to zero absorption value, we can obtain the band gap energy is equal to 3.24 eV. This value seemed to a little deviate from the theoretical value of 3.3 eV, however, it was agreed with the exciton energy of ZnO ( $E_b=60$  meV). We thought the result may be caused by the closing between two energy levels, so the energy band appeared to be continuous. Thus we obtained the exciton energy. Besides, there is a long-range band tailing region extending tens nanometer, found 420 nm was located in the band tailing region, so saturation absorption of band tailing defect states would be observed. As laser intensity increased, the behavior of saturation absorption gradually disappeared, indicating TPA and FCA effects become dominant. From our results, we should tune our input intensity higher than  $0.63$  GW/cm<sup>2</sup> to avoid the influence of band tailing at 420 nm. Notice that although 390 nm is also located in this region, the wavelength is much closed to the band gap energy as compared with 420 nm, so the contribution of FCA is greater than that of band tailing defect even under low input density.

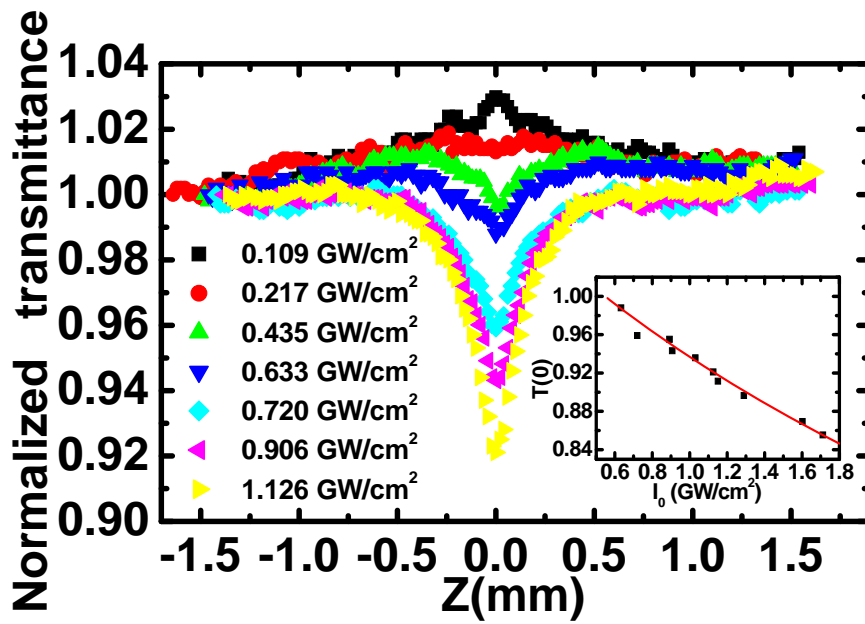


Fig. 4-8 Open aperture z-scan traces of ZnO thin film under different input intensity at 420 nm. The inset is the nonlinear transmission measurement at focal point, which is the position of Z=0.

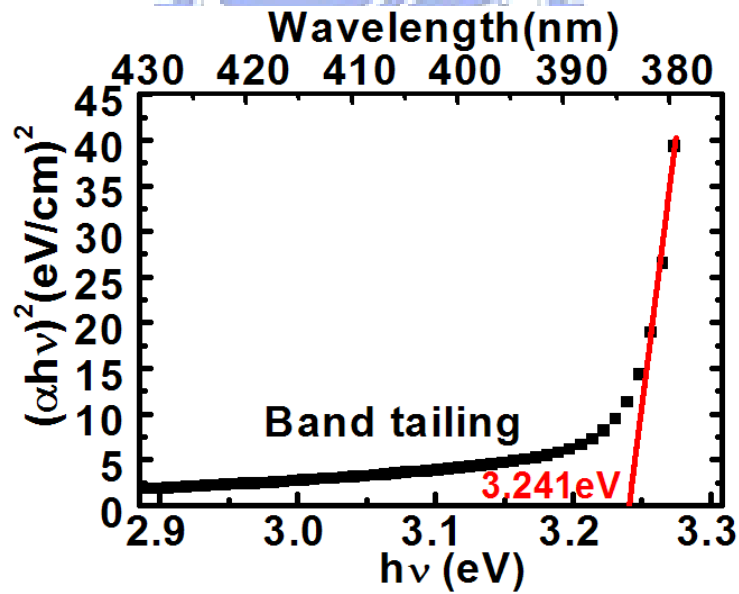


Fig. 4-9 Plot of  $(\alpha h\nu)^2$  versus energy

With the same process described at 390 nm, a plot of effective two photon coefficient  $\beta_{eff}$  versus input intensity at 420 nm is shown in Fig. 4-11. To investigate the mechanism

of nonlinear absorption under near-exciton resonance region, the calculated results between 390 nm and 420 nm were also presented in Fig. 4-11. Wavelength-dependent variation was observed in this figure. Notice that the effective TPA coefficient here actually contains three components that can be expressed as

$$\beta_{eff} = \beta + DI = \left( \beta_0 + \frac{\sigma_a \alpha_0 \tau_p}{\hbar \omega} \right) + \frac{\sigma_a \beta_0 \tau_p}{2\hbar \omega} I = \beta_0 + \beta_1 + \beta_2, \quad (4-1)$$

where  $\beta_0$ ,  $\beta_1$ , and  $\beta_2$  represent the contributions of intrinsic TPA, FCA induced by one photon absorption, and FCA induced by two photon absorption, respectively. The deductive processes were discussed in detail in Chapter 2. When the pump wavelength was very close to the band gap energy of ZnO, the pump energy was high enough to excite a large number of electrons into conduction band by TPA, so the probability of FCA increased obviously. Therefore, the linear relationship was displayed and the slope increased evidently with decreasing wavelength. As the investigated wavelength moved away from the band gap energy,  $\beta_{eff}$  would finally become a constant, which illustrated the third-order nonlinearity caused from TPA was the main nonlinear mechanism.

In Fig. 4-11(b), we also observed departures under low intensity.  $\beta_{eff}$  were smaller than the expected values, which were along the straight line under high intensity. The phenomenon was resulted from the linear absorption saturation of band tailing defect states. Because absorption saturation would function as an effective negative TPA coefficient, then the net value of effective TPA coefficient was reduced. However, the influence could be



neglected at higher intensity. This reason also accounted for the queer effect under low intensity at 410 nm and 420 nm. Figure 4-10 shows the comparison of open aperture Z-scan measurements with different wavelengths under an input irradiance of 0.1 GW/cm<sup>2</sup>. As we tuned the laser toward shorter wavelength, the stronger saturation behavior was observed due to closing to the band edge in band tailing region, which could also be proved in Fig. 4-9. Following the same fitting procedure mentioned previously, the magnitude of  $\beta_{eff}$  can be obtained to be -5419 (cm/GW) and -3118 (cm/GW) at 410 nm and 420 nm, respectively. Thus, at low pump intensity, the reduction at 410 nm was greater than that at 420 nm in Fig 4-11(b). For this reason, the initial magnitude of  $\beta_{eff}$  at 410 nm at low intensity was smaller than that at 420 nm. When the input intensity increased, the contribution of TPA and FCA became large, so  $\beta_{eff}$  in the use of 410nm is larger than that in the use of 420nm.

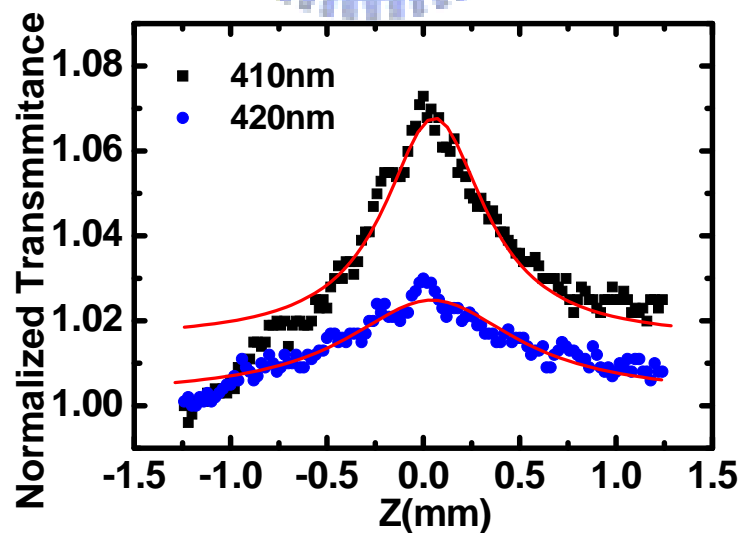


Fig. 4-10 Wavelength dependence of open aperture Z-scan at input irradiance of 0.1GW/cm<sup>2</sup>.

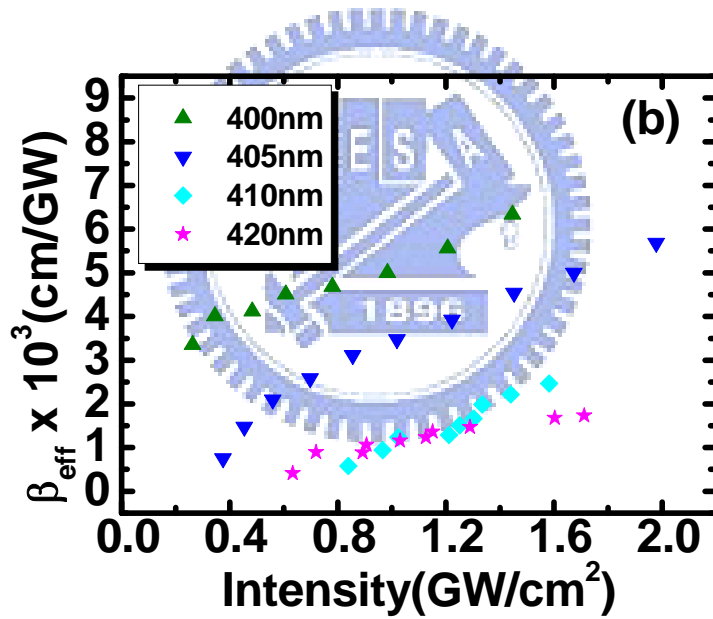
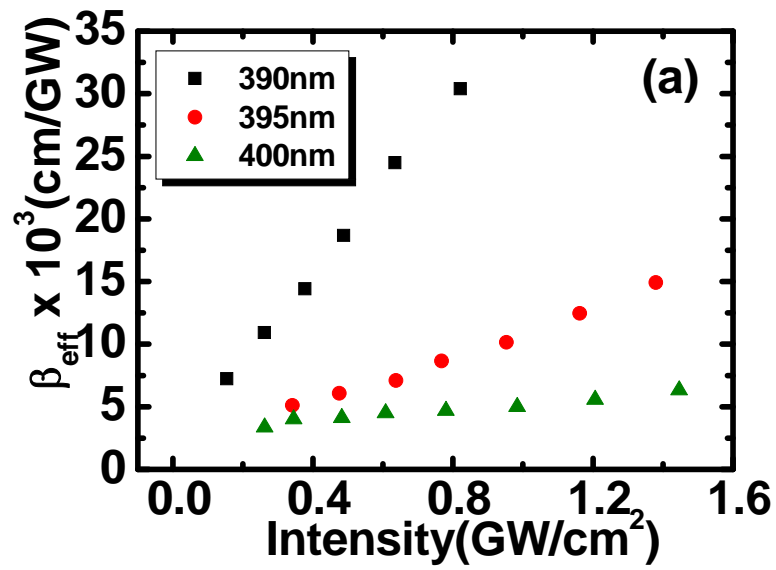


Fig. 4-11 Variation of effective two photon absorption coefficient with input intensity at different wavelengths.  
 (a) 390 nm-400 nm (b) 400 nm-420 nm

Here we present the procedure to obtain the intrinsic TPA coefficient instead of effective TPA coefficient. From Eq. (4-1), we know the intercept of the slope with the vertical axis in Fig. 4-11 not only include the contribution of the intrinsic TPA but also include FCA caused

by the linear absorption. To separate these two items we need the information of  $\sigma_a$  and  $\beta_0$  given from the value of slope  $D = \frac{\sigma_a \beta_0 \tau_p}{2\hbar\omega}$ . However, the fitted value of slope would vary depending on the number of data we choose. To avoid this situation and acquire the intrinsic TPA coefficient more accurately, we utilize nonlinear transmission measurement at focal point, which is at the position of  $Z=0$ . From the open aperture Z-scan traces at different intensities, we easily yield the dependence of the nonlinear transmission  $T(0)$  on the input irradiance  $I_0$ , as illustrated by squares in the inset of Fig. 4-8. This figure is fitted by using Eq. (2-24) with two parameters to extract both  $\beta$  and  $D$ . The fitted values showed in the inset of Fig. 4-8 by the solid lines indicating  $\beta=604$  (cm/GW) and  $D=0.21$  (cm<sup>3</sup>/GW<sup>2</sup>) at 420 nm, from which we can use the following two formula

$$\beta = \beta_0 + \frac{\sigma_a \alpha_0 \tau_p}{\hbar\omega}, \quad (4-2)$$

$$D = \frac{\sigma_a \beta_0 \tau_p}{2\hbar\omega} \quad (4-3)$$

to evaluate the cross-section of free carrier absorption  $\sigma_a$  and intrinsic TPA coefficient  $\beta_0$  by taking the pulse width  $\tau_p$  to be 200 fs. Table IV lists other calculated values between 390 nm and 420 nm. To examine the contribution of  $\beta_2$ , we obtain the value of  $\beta_2$  by the multiplication of  $D$  and intensity  $I$ , and here we use the value of  $I$  to be equal to 1.6 GW/cm<sup>2</sup>. From the table, we know the contribution of FCA induced by both the linear absorption  $\beta_1$  and TPA  $\beta_2$  was puny compared with  $\beta_0$  due to the small value of  $\sigma_a$  and  $D$ . We also found  $\beta$  at 390 nm in Table IV was larger than that by using the intercept of the fitted line

with y axis shown in Fig. 4-7. Although the values which used two fitting methods were different, the order of two values was the same. The increasing tendency of the slope as pump wavelength became shorter in Fig. 4-11(b) was consistent with the tendency of D in Table IV. Besides,  $\sigma_a$  is at the same order by using different pump wavelength in Table IV and it means cross section of free carrier is nearly wavelength independent. Although  $\sigma_a$  varied a little during the investigated regime, we think it may result from large errors in fitting when wavelength approach band edge.

Table IV. Fitted and calculated coefficients in nonlinear transmission measurements between 390 nm and 420 nm.

Wavelength (nm)	$\beta$ (cm/GW)	$D$ (cm <sup>3</sup> /GW <sup>2</sup> )	$\beta_0$ (cm/GW)	$\sigma_a$ (10 <sup>-18</sup> cm <sup>2</sup> )	$\beta_1$ (cm/GW)	$\beta_2$ (cm/GW)
390	2990	2.94	2975	5.04	15	4.70
395	1663	1.26	1651	3.85	12	2.02
400	940	0.38	934	2.03	6	0.61
405	829	0.24	825	1.44	4	0.38
410	780	0.23	775	1.43	5	0.37
420	604	0.21	599	1.64	5	0.34

In order to investigate the complete variation of TPA coefficient of ZnO thin film in near-UV and IR region, we review some results of Lin et al. in *J. Appl. Phys.* **Vol.97,033526** (2005) [14]. Figure 4-12 shows the combined results, in which the open squares represent previous result while the solid squares represent ours. The previous observation was based

on the resonance of exciton energy with twice the incoming photon energy, which was obvious in Fig. 4-12, in which an enhancement at 760 nm corresponding to  $(E_g - E_b)/2$  of ZnO was observed. Here we observed that the excitonic state can also enhance the nonlinear absorption at the same exciton transition energy, rather than one-half of exciton transition energy. When pump wavelength approached to 383 nm, which is the exciton resonance proved in Fig. 4-9, we observed  $\beta_0$  increased rapidly. The enhancement order was even higher than that at one-half exciton energy. This near-exciton enhancement behavior have been seen in GaN thin films [18]. In the GaN thin film, the peak value of two photon absorption coefficient is 1500 (cm/GW) which reveals an enhancement factor  $> 100$  than the values of 15 (cm/GW) at off-resonance region. Consequently, comparing with the results in reference, in which  $\beta_0 = 4.2 \text{ cm/GW}$  was measured in 1mm ZnO single crystal at a pump wavelength of 532 nm [13], and with our previous results [14], we found TPA coefficient of ZnO would be enhanced by a factor of 120 at one-half exciton energy and enhance more than a factor of 710 at near exciton resonance.

Summing up the effects mentioned above and inspecting  $D = \frac{\sigma_a \beta_0 \tau_p}{2\hbar\omega}$  term once again, it is clear now that with enhanced  $\beta_0$  at near-exciton resonance, FCA would becomes evident as compared with those of off-resonance.

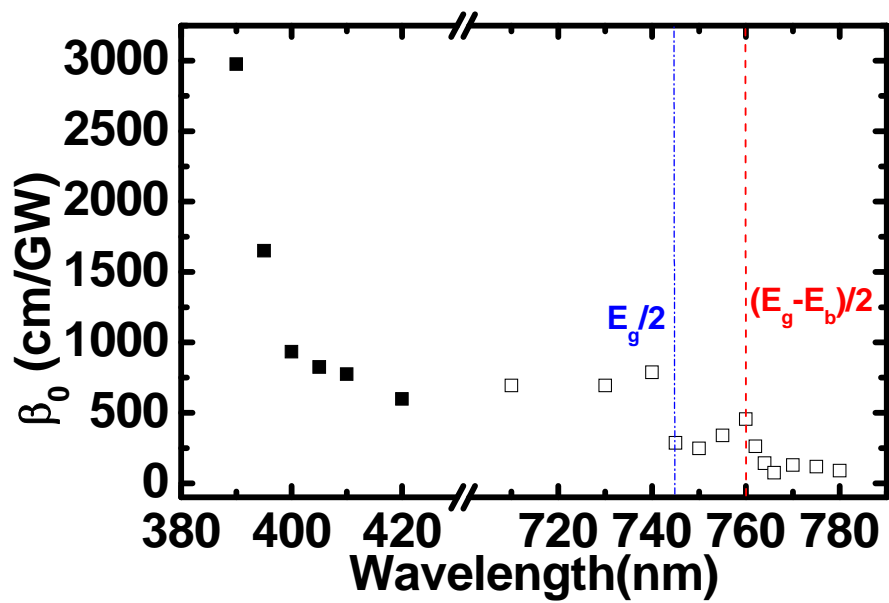
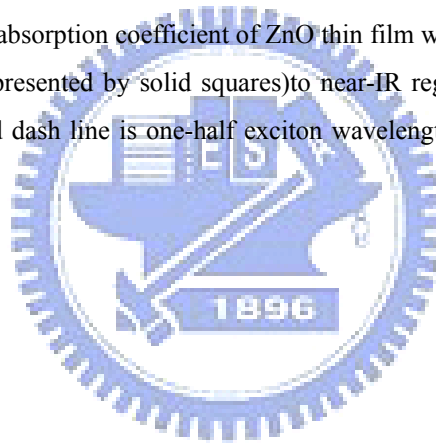


Fig. 4-12 Variation of two photon absorption coefficient of ZnO thin film with pump wavelength extending from near-UV (our results represented by solid squares) to near-IR region (previous results represented by open squares). The red dash line is one-half exciton wavelength, and the blue dash line is one-half band gap energy.



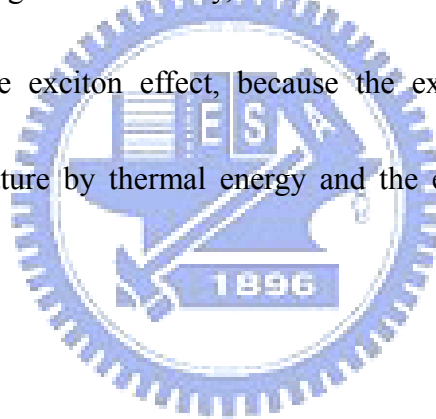
## Chapter 5 Conclusions and Perspectives

### 5-1 Conclusions

The variation of near resonant high-order optical nonlinearities of ZnO thin film made by the laser MBE were investigated by the Z-scan method using the high repetition rate femtosecond Ti:sapphire laser with doubled-frequency wavelength which is tuned from 390 nm to 420 nm. Our ZnO thin film is c-axis orientation and well-crystalline with a strong free-exciton luminescence at 380 nm that is demonstrated by the XRD and room temperature PL, respectively. We observed an enormous enhancement of TPA coefficient due to near-exciton resonance. When photoexcitation energy is close to exciton transition energy, the TPA coefficient is about 3000 cm/GW, which is 710 times larger than that of ZnO bulk measured at 532 nm. The order of enhancement is even greater than that in near-IR regime. In addition, the higher order nonlinearity, FCA, becomes evident in the near band edge region due to the enhanced TPA coefficients. As a result, a modified method, which considered higher nonlinearity, was used in our experimental results and the calculated values were sensible. Nevertheless, after considering the contributions of every possible mechanism, we found nonlinear absorption mainly resulted from TPA. Besides, the effects of band tailing states on nonlinear absorption were also observed under low input intensity through z-scan method.

## 5-2 Perspectives

In our measurements, the used shortest wavelength was 390 nm. With wavelength shorter than 390 nm, the transmittance was too low to measuring by Z-scan. In order to investigate the behavior of TPA coefficient at pump photon energy which is at or even above the exciton energy, using pump-probe technique is needed. Besides, we focus nonlinear absorption in the thesis. As reported in Ref [14], to further study the behavior of nonlinear refractive index in the near-resonant regime we should reduce thermal influence by lowering the repetition rate of exciting laser. Finally, a series of temperature dependent Z-scan is necessary for inspecting the exciton effect, because the exciton binding energy will be destroyed at higher temperature by thermal energy and the enhanced nonlinearities at low temperature may decrease.





## References

- [1] T. Pertsch, U. Peschel, and F. Lederer, "All-optical switching in quadratically nonlinear waveguide arrays," *Optics Letters*, vol. 28, pp. 102-104, Jan 2003.
- [2] K. M. Fryad Z. Henari, and Werner J. Blau, Vladimir A. Karavanskii and Vladimir S. Dneprovskii, "Third-order optical nonlinearity and all-optical switching in porous silicon," *Applied Physics Letters*, vol. 67, p. 3, 1995.
- [3] R. W. Boyd, *Nonlinear Optics*, 1992.
- [4] A. A. S. MANSOOR, SHEIK-BAHAEE, TAI-HUEI WEI, DAVID J. HAGAN, E. W. VAN STRYLAND, "Sensitive Measurement of Optical Nonlinearities Using a Single Beam," *IEEE JOURNAL OF QUANTUM ELECTRONICS*, vol. 26, p. 10, 1990.
- [5] M. H. Huang, S. Mao, H. Feick, H. Q. Yan, Y. Y. Wu, H. Kind, E. Weber, R. Russo, and P. D. Yang, "Room-temperature ultraviolet nanowire nanolasers," *Science*, vol. 292, pp. 1897-1899, Jun 2001.
- [6] Y. F. C. D. M. Bagnall, Z. Zhu, T. Yao, M. Y. Shen and T. Goto, "High temperature excitonic stimulated emission from ZnO epitaxial layers," *Applied Physics Letters*, vol. 73, p. 3, 1998.
- [7] Z. K. Tang, G. K. L. Wong, P. Yu, M. Kawasaki, A. Ohtomo, H. Koinuma, and Y. Segawa, "Room-temperature ultraviolet laser emission from self-assembled ZnO microcrystallite thin films," *Applied Physics Letters*, vol. 72, pp. 3270-3272, Jun 1998.
- [8] S. K. S. Gregory and J. Exarhos, "Influence of processing variables on the structure and properties of ZnO films," *Thin Solid films*, vol. 270, p. 6, 1995.
- [9] U. Ozgur, Y. I. Alivov, C. Liu, A. Teke, M. A. Reshchikov, S. Dogan, V. Avrutin, S. J. Cho, and H. Morkoc, "A comprehensive review of ZnO materials and devices," *Journal of Applied Physics*, vol. 98, p. 103, Aug 2005.
- [10] H. Cao, J. Y. Wu, H. C. Ong, J. Y. Dai, and R. P. H. Chang, "Second harmonic generation in laser ablated zinc oxide thin films," *Applied Physics Letters*, vol. 73, pp. 572-574, Aug 1998.
- [11] G. Wang, G. T. Kiehne, G. K. L. Wong, J. B. Ketterson, X. Liu, and R. P. H. Chang, "Large second harmonic response in ZnO thin films," *Applied Physics Letters*, vol. 80, pp. 401-403, Jan 2002.
- [12] G. I. Petrov, V. Shcheslavskiy, V. V. Yakovlev, I. Ozerov, E. Chelnokov, and W. Marine, "Efficient third-harmonic generation in a thin nanocrystalline film of ZnO," *Applied Physics Letters*, vol. 83, pp. 3993-3995, Nov 2003.
- [13] X. J. Zhang, W. Ji, and S. H. Tang, "Determination of optical nonlinearities and carrier lifetime in ZnO," *Journal of the Optical Society of America B-Optical Physics*, vol. 14, pp. 1951-1955, Aug 1997.
- [14] J. H. Lin, Y. J. Chen, H. Y. Lin, and W. F. Hsieh, "Two-photon resonance assisted huge nonlinear refraction and absorption in ZnO thin films," *Journal of Applied Physics*, vol. 97, p. 6, Feb 2005.
- [15] L. L. C. Robert Adair, Stephen A. Payne, "Nonlinear refractive index of optical crystals," *Physical Review B*, vol. 39, p. 14, 1989.
- [16] Z. W. Dong, C. F. Zhang, G. J. You, X. Q. Qiu, K. J. Liu, Y. L. Yan, and S. X. Qian, "Multi-photon excitation UV emission by femtosecond pulses and nonlinearity in ZnO single crystal," *Journal of Physics-Condensed Matter*, vol. 19, p. 7, May 2007.

- [17] Y. B. Han, J. B. Han, S. Ding, D. J. Chen, and Q. Q. Wang, "Optical nonlinearity of ZnO microcrystallite enhanced by interfacial state," *Optics Express*, vol. 13, pp. 9211-9216, Nov 2005.
- [18] K. H. Lin, G. W. Chern, Y. C. Huang, S. Keller, S. P. DenBaars, and C. K. Sun, "Observation of huge nonlinear absorption enhancement near exciton resonance in GaN," *Applied Physics Letters*, vol. 83, pp. 3087-3089, Oct 2003.
- [19] M. S.-B. A. A. Said, D. J. Hagan, T. H. Wei, J. Wang, J. Young, and E. W. Van Stryland, "Determination of bound-electronic and free-carrier nonlinearities in ZnSe, GaAs, CdTe, and ZnTe," *Journal of the Optical Society of America B*, vol. 9, 1992.
- [20] C. H. K. H.P. Li, Y.L. Lam, W. Ji, "Optical nonlinearities and photo-excited carrier lifetime in CdS at 532 nm," *Optics Communications*, vol. 190, p. 6, 2001.
- [21] B. Gu, W. Ji, P. S. Patil, S. M. Dharmaparakash, and H. T. Wang, "Two-photon-induced excited-state absorption: Theory and experiment," *Applied Physics Letters*, vol. 92, p. 3, Mar 2008.
- [22] T. Y. W. a. T. Ohmura, *Quantum theory of scattering*, 1962.
- [23] J. G. J. C. Manificier, and J. P. Fillard "A simple method for the determination of the optical constants, n, k and the thickness," *Journal of Physics E*, vol. 9, p. 3, 1976.
- [24] J. Thomas, M. Anija, J. Cyriac, T. Pradeep, and R. Philip, "Observation of a fifth order optical nonlinearity in 29 kDa Au@alkanethiol clusters excited in the visible," *Chemical Physics Letters*, vol. 403, pp. 308-313, Feb 2005.
- [25] L. Irimpan, A. Deepthy, B. Krishnan, V. P. N. Nampoore, and P. Radhakrishnan, "Nonlinear optical characteristics of self-assembled films of ZnO," *Applied Physics B-Lasers and Optics*, vol. 90, pp. 547-556, Mar 2008.
- [26] B. L. Yu, C. S. Zhu, F. X. Gan, X. C. Wu, G. L. Zhang, G. Q. Tang, and W. J. Chen, "Optical nonlinearities of Fe<sub>2</sub>O<sub>3</sub> nanoparticles investigated by Z-scan technique," *Optical Materials*, vol. 8, pp. 249-254, Nov 1997.
- [27] H. P. Li, C. H. Kam, Y. L. Lam, and W. Ji, "Optical nonlinearities and photo-excited carrier lifetime in CdS at 532 nm," *Optics Communications*, vol. 190, pp. 351-356, Apr 2001.
- [28] M. S. F. yakuphanoglu, O. F. Ozturk, "The determination of the optical constants of Cu(II) compound having 1-chloro-2,3-o-cyclohexylidinepropane thin film," *optics Communications*, vol. 239, p. 6, 2004.